

Improving Energy Recovery in Blended Antilock Braking Systems of Electric Vehicles

Andrei Aksjonov
ŠKODA AUTO a.s.
Mladá Boleslav, Czech Republic
andrei.aksjonov@skoda-auto.cz

Valery Vodovozov and Zoja Raud
Tallinn University of Technology
Tallinn, Estonia
valery.vodovozov@ttu.ee

Abstract — Considering highest demands continually imposed on equipment indispensable for safe transportation, this paper focuses on on-board controllers for blended (electro-hydraulic) antilock braking systems of road electric vehicles. Recommendations are issued regarding an influence of air friction and road inclination on torque allocation between electric and hydraulic brakes and accurate accounting of the hybrid energy storage. Following the study of three types of controllers – PID, tabular, and fuzzy logic – the latter one was offered as the most efficient solution for equally fast and safe braking with maximal energy recovery on different roads, from dry to icy, without locking and skidding even in critical situations. Several parts of the system were explored in case studies ensuring their validity and accuracy.

Keywords — *on-board controller; road electric vehicle; antilock braking system; blended braking system; fuzzy logic.*

I. INTRODUCTION

Though the worldwide total of electric vehicles (EV) fed by electrical drives (ED) has overcome two million in 2017, it turned out to be about an order of magnitude less than was forecasted [1], primarily because of environmental consequences. Nowadays EVs are recharged by electricity, two-thirds of which is originated from the combustion of fossil fuels. Inter alia, French EVs are largely nuclear-fission cars, whereas in India, China, and Poland EVs are overwhelmingly coal cars, and the like. Even in the case of renewable sources, much greenhouse gases are emitted during the production of cement and steel for hydroelectric stations, wind turbines, and photovoltaic panels. Besides, EV manufacturing itself creates three times higher toxicity as it does for conventional cars [1].

In reply, new approaches are manifested now in EV development. To reduce specific electricity consumption, hybrid energy storage systems (HESS) are introduced that combine the high energy density part (battery) and high power density part (ultracapacitors and/or flywheels) [2], [3]. Likewise, taking in mind that from 15 to 50% of the urban driving energy is consumed in braking [4], blended (electro-hydraulic) braking systems are promoted. Along with traditional hydraulic brakes (HB) they envisage electric braking (EB), or recuperation, which provides energy recovery that might benefit in fuel economy and growth of the braking efficiency [5], [6]. Based on these trends, a new generation of antilock braking systems (ABS) arises that consolidate HB and EB features in both the gradual and the critical braking situations.

Despite the potential advantages of blended ABS, many EV manufacturers still choose HB as a default priority due to the low efficiency of EB (20 to 35% [6], [7]) resulting, in particular, from following design circumstances:

- vagueness of EV models used for braking torque accounting due to such instable and uncertain factors as air friction, road inclination, etc. [2], [3], [8] – [10];
- excluding ABS and HESS specificity from consideration of torque distribution between front and rear wheels and between HB and EB [3], [8], [10], [11];
- neglecting continuously changing tire properties and road surface variations [3], [8], [10];
- simulation without experimental validation of offered models and strategies [2], [3], [6] – [10], [12], [13].

In this paper, some ways to improve energy recovery are proposed. First, recommendations are made on considering an influence of air friction and road inclination on braking torque. Second, more accurate accounting of constraints from ED and HESS sides is produced. Herewith, three versions of controllers for HESS-oriented blended ABS are compared – PID, tabular, and fuzzy logic – aiming to recommend the best solution in view of energy saving.

The research fits the hierarchical system topology [2], [9], [14] with ideal braking force distribution between front and rear wheels [3], [10] according ECE-R13 Regulation [15]. The concern is to the dynamics model and HESS model clarifications as well as torque allocation with an objective to analyse the effect of such features as energy recovery, system robustness to different road surfaces, and vehicle handling, assuming that recuperation is not deactivated, keeping priority even in critical situations, specifically with ABS.

II. BRAKING DYNAMICS OF ELECTRIC VEHICLES

To slow down the EV from an initial velocity v by capturing vehicle energy W_B within some given time interval t , appropriate braking power P_B and force F_B have to be applied:

$$W_B = \int P_B dt = v \int F_B dt. \quad (1)$$

In compliance with [16], [17], dynamics of the braking system are determined by

$$ma = F_B \quad (2)$$

where

m – total EV mass;

$a = -\frac{dv}{dt}$ – EV longitudinal deceleration.

The braking force (longitudinal road friction) has to withstand air friction F_{air} , climbing friction F_g , and rolling friction F_r :

$$F_B = F_{air} + F_g + F_r. \quad (3)$$

Air resistance is given in [18], [19] by

$$F_{air} = 0.5\rho C_{air}Q(v \pm v_{wind})^2 \quad (4)$$

where

ρ – air density;

C_{air} – aerodynamic drag coefficient;

Q – EV front area;

v_{wind} – wind velocity.

The climbing force resists the EV to climb an inclination as follows:

$$F_g = mg \sin(\beta) \quad (5)$$

where

g – acceleration due to gravity;

β – climbing slope.

Essential nonlinearity, time variability, and uncertainty of braking dynamics take place mainly due to the rolling friction force,

$$F_r = \mu mg \cos(\beta) \quad (6)$$

where μ is tire-road friction factor known also as an adhesive coefficient.

To produce the braking force (2), proper braking torque T_B and power P_B have to be applied:

$$T_B = F_B r, \quad (7)$$

$$P_B = T_B \omega_w \quad (8)$$

where

r – wheel effective radius;

ω_w – angular speed of a wheel.

To evaluate how power components – such as aerodynamic power P_{air} , rolling power P_r , and climbing power P_g – affect the braking power (8) at different EV velocities, simulation has been conducted on straight (a) and 20° downhill (b) roads. An electric car with $m=1500$ kg, $Q=3$ m², $r=0.3$ m, $\rho=1.2$ kg/m³, $C_{air}=0.5$ was studied at gradual ($\mu=0.1$) and critical ($\mu=1$) braking situations.

At gradual braking with no inclination (Fig. 1a), the rolling force (P_r) dominates only at the low velocity whereas at rapid cruising the significant part of power is spent to overcome the air resistance (P_{air}). On an inclination (Fig. 1b), much power is directed to overcoming the climbing counterforce (P_g).

At critical braking (Fig. 2), the rolling force (P_r) always predominates, both on longitudinal (Fig. 2a) and inclination (Fig. 2b) driveways. However, until the adhesive coefficient approaches its top level, it passes all intermediate levels, from 0.1 to 1, as well as all velocities, from initial to zero. It

means, to accurately evaluate the braking force, both the alternating vehicle velocity and the variable adhesion have to be taken into account.

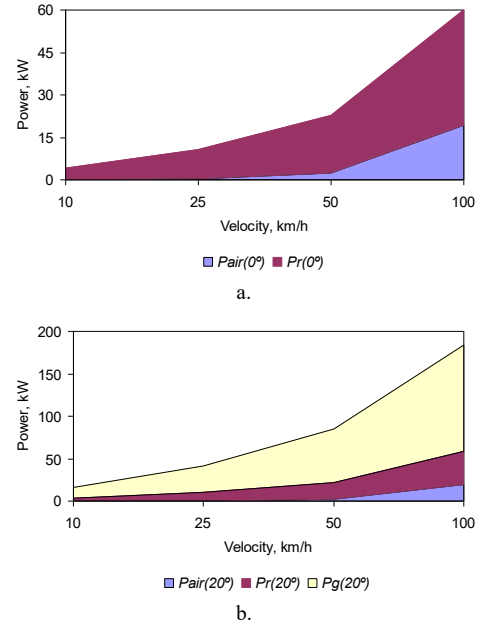


Fig. 1. Braking power components at gradual braking, $\mu = 0.1$.

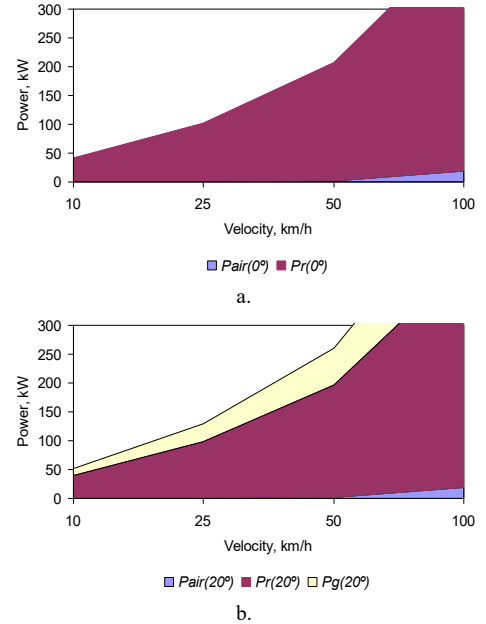


Fig. 2. Braking power components at critical braking, $\mu = 1$.

As a rule, the adhesive coefficient can be found experimentally or via simulation without climbing and wind using (2) – (6):

$$\mu = \frac{ma - 0.5\rho C_{air}Qv^2}{mg}. \quad (9)$$

Only at a point of maximal adhesion, air friction may be neglected and the commonly used simplification [20] is valid,

$$F_B = \mu mg. \quad (10)$$

In that case,

$$\mu = \frac{ma}{mg} = \frac{a}{g}. \quad (11)$$

III. BRAKING TORQUE ALLOCATION

The studied model of the EV braking (Fig. 3) consists of four modules: Driver, Electronic Control Unit (ECU, or controller), HESS, and blended ABS involving EB and HB blocks.

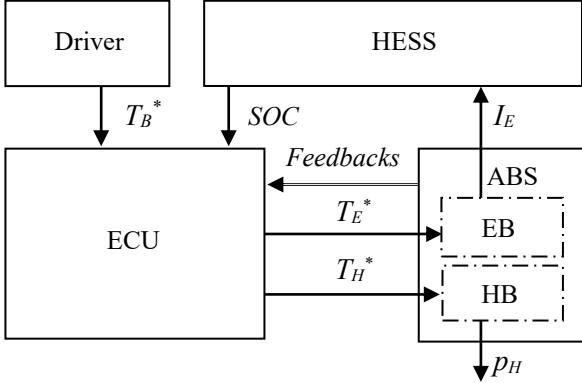


Fig. 3. The model of EV braking.

Once the driver pushes the brake pedal, the pedal displacement signal T_B^* comes from the driver to the ECU. The state-of-charge (SOC) signals from HESS and the *Feedbacks* from EV sensors serve as ECU inputs as well. From ECU, computed EB and HB torque commands T_E^* , T_H^* go to the appropriate ABS inputs whereas the current I_E recharges HESS from EB and pressure p_H adjusts the HB. Braking continues until pedal releasing.

The ECU performs three functions: (a) T_B^* evaluation and conversion to the permissible torque reference T^* ; (b) T^* distribution between the front and rear wheels; (c) T^* allocation between HB and EB. To undertake the first function (a), the pedal displacement T_B^* is analysed. At little T_B^* , the gradual braking mode is identified, whereas at heavy effort, braking is recognised as critical.

The second function (b), not detailed in this paper, is executed according the ECE-R13 Regulation [15] as a fixed ratio calculated from the EV dynamics (2) – (11). At normal EV design, the maximal power, which ED can develop, $P_{ED \max}$, corresponds to the traction power (8) at the maximal velocity and adhesion $\mu \leq 0.1$. In turn, during the gradual braking the required adhesive coefficient may be either below or above this value, whereas at critical braking adhesion approaches 1.

As for the third function (c), to allocate torque competently between EB and HB, the premise is that the ED has enough capacity to charge either of the HESS parts, that is:

$$\begin{aligned} P_{ED \max} &> \{P_{UC \max} \vee P_{BAT \max}\} \\ U_{ED \max} &> \{U_{UC \max} \vee U_{BAT \max}\} \\ I_{ED \max} &> \{I_{UC \max} \vee I_{BAT \max}\} \end{aligned} \quad (12)$$

where

$U_{ED \max}$, $I_{ED \max}$ – maximal voltage and current of the ED;

$P_{UC \max}$, $U_{UC \max}$, $I_{UC \max}$, $P_{BAT \max}$, $U_{BAT \max}$, $I_{BAT \max}$ – maximal power, voltage, and current of the ultracapacitor and the battery, respectively;
 \vee – maximum operator.

On the other hand, to keep the ultracapacitor and the battery inside the safe margins at any instant, torque T_E^* and current I_E of the ED have to be limited by the real-time HESS conditions, namely, SOC_{UC} and SOC_{BAT} [13], [21]:

$$T_E^* = I_E \psi = \{I_{UC}(SOC_{UC}) \psi \vee I_{BAT}(SOC_{BAT}) \psi\} \quad (13)$$

where I_{UC} , and I_{BAT} are the real-time recharging currents of the ultracapacitor and battery and ψ is the ED flux linkage.

The remaining fraction of required braking torque is requested from the HB:

$$T_H^* = T^* - T_E^*. \quad (14)$$

To adjust desired HB torque, HB pressure p_H is regulated as follows:

$$p_H = k_H \cdot T_H^* \quad (15)$$

where k_H is a fixed HB coefficient.

Fig. 4 demonstrates the appropriate torque allocation strategy.

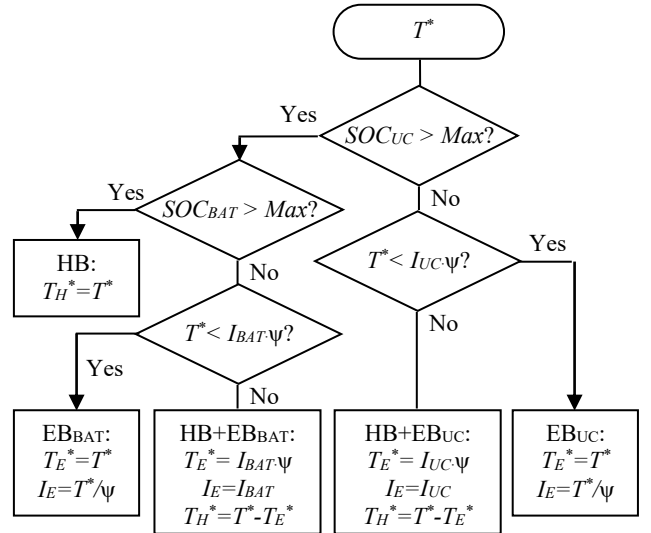


Fig. 4. The flowchart of braking torque allocation.

While both SOC levels overcome permissible overcharging barriers (Max), the sole HB is used due to recuperation impossibility. Once one or both SOC s drop, EB_{UC} or EB_{BAT} comes into play being acted alone until ED torque becomes insufficient to maintain the reference T^* . In the latter case, conventional for ABS, the ECU runs both HB and EB ($HB+EB_{UC}$ or $HB+EB_{BAT}$).

A particular strength of this strategy is the ability to use EB in most situations, including critical braking.

Three widely used control methods were investigated by simulation and experimentation in view of their suitability for safe braking with maximal energy recovery on different roads: closed-loop (PID and sliding), piecewise (tabular), and fuzzy logic control (FLC).

IV. PID AND SLIDING CONTROLLERS

Examples of PID controllers, including the sliding mode ones, are presented in [5], [9], [13], [22]. In Fig. 5, the studied model is shown. Here, the feedback signals T_H , T_E from appropriate sensors compose real-time torque T and, after the comparison with the requested T_B^* level, the error ΔT is converted by the controller to T^* and directed to the torque allocation module, which algorithm is displayed in Fig. 4. Once T_B^* exceeds T , the sliding-mode controller saturates. Otherwise, as T overcomes T_B^* , the controller desaturates thus stabilizing the torque level. Such releasing and applying of brakes may happen every 4 to 400 ms (2.5 – 250 Hz) depending on ABS and EV models [5], [16].

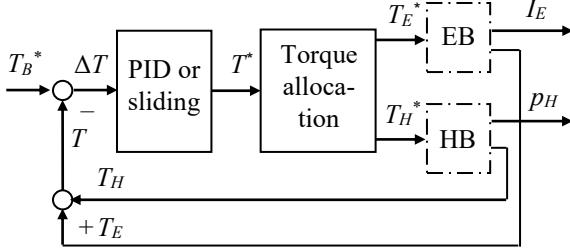


Fig. 5. PID and sliding control.

The benefits of the PID control are structural simplicity, standard tuning procedures, and suitability for adjusting. Its drawbacks are low accuracy at fragile and unclear road conditions, requirements in sensors for torque estimation, and impossibility to support equally high braking rate with time. As follows from [22], the sliding mode produces oscillations in control signal that can cause system instability and damage to the actuators. Because of braking torque ripple, the system performance is degraded due to the torque limitation and actuator delays. Particularly for this reason, in [6] the sliding mode is used for the HB control only. Another important problem of this controller is its unsuitability for ABS.

V. TABULAR CONTROLLER

To manage ABS, the ECU has to be responsible for not only torque allocation, but also for maintaining the tractive contact between the wheels and the road surface, preventing wheels from locking, and avoiding uncontrolled skidding. To apply braking torque upon the maximal adhesive coefficient without torque sensors, longitudinal wheel slip λ is to be considered, i.e. the relative motion of a wheel over the road:

$$\lambda = \frac{v - \omega_w r}{v} \quad (16)$$

The ABS-oriented blended braking systems were simulated by the authors in [23] and experimentally studied in [24].

Initially, vehicle braking has been modelled on dry, wet, damp, and icy road surfaces without ABS. Simulation was conducted in the HB simulator of the four-in-wheel-drives (4WD) sport utility car designed and parameterized in accordance with the specifications provided by the manufacturer. The control algorithm was developed in Automotive Simulation Models™ (ASM™) offered by

dSPACE® GmbH Software 2014-B (64-bit, Paderborn, Germany) and interacted with MATLAB®/Simulink® R2013b (64 Bit, Natick, MA, USA). While the simulator adjusted the front and rear wheels, tires were modelled with the Pacejka's Magic Formula [25]. The obtained traces of the adhesive coefficients versus wheel slip are shown in Fig. 6. These data were further used by the ECU to maintain the optimal slip level, at which, due to the high braking force, the EV is capable to decelerate as fast as feasible.

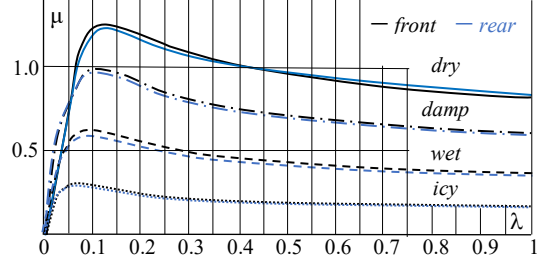


Fig. 6. The adhesive coefficient for various road surfaces and wheel slip estimated in [23].

Next, the full 10-degree-of-freedom (10DOF) EV model has been developed and parameterized, where each of 4WD powertrain EDs was connected to the appropriate wheel through a half-shaft transmission. Both the HB affecting braking pressure and the EB generating the recharging current were adjusted independently. Torque blending and recuperation capability were studied for every wheel. The control algorithm was designed in the ASM™ toolkit interacted with MATLAB®/Simulink®.

To bring slip into conformity with an appropriate adhesive coefficient, the EV model has been subjected to learning. During the learning procedure, the EV was preliminary running on dry, wet, damp, and icy road surface imitators under heavy braking conditions with locked wheels. As a result, a set of timing diagrams was acquired (Fig. 7) that demonstrates EV decelerations on the explored roads. Using (9) or (11), these traces may be used to estimate the adhesion curve of the corresponding road.

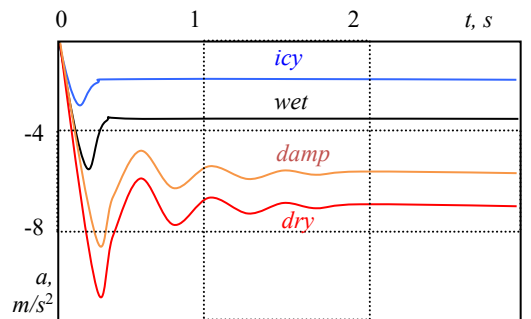


Fig. 7. ED deceleration traces for various road surfaces performed with locked wheels.

The physical setup used for model parts validation is described in [24]. It represents the quarter-vehicle imitator driven from the MATLAB®/Simulink® interface via the Real-Time Window Target™ Toolbox and MATLAB® (Natick, MA, USA) Fuzzy Logic Toolbox™. The test rig developed

by Inteco® Ltd. (Krakow, Poland) for the HB study includes two wheels. The first wheel used as the EV wheel speed source was decelerated by friction applied through a disc braking system. Another, ED-fed wheel imitating the car velocity source, rotated the first one with a certain speed.

Using the above results, the tabular ABS-oriented ECU was designed (Fig. 8). It implies the slip analyse, road analyse, lookup table, and torque allocation.

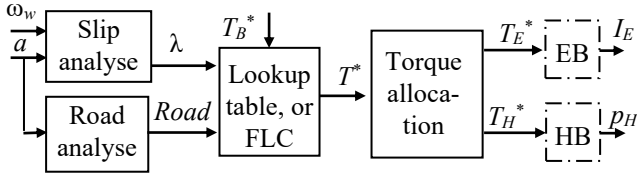


Fig. 8. Tabular and fuzzy logic ABS-oriented control.

To estimate real-time slip with the help of (16), wheel speed and vehicle deceleration signals are acquired from appropriate built-in vehicle sensors. To detect the road surface with the help of (9) or (11), the vehicle deceleration signal is compared with extremes from Fig. 7. The results of the slip and road analyses come to the lookup table representing the tabular image of Fig. 6. For the front wheels, it looks like Table I, where 1.0, 0.8, 0.6, 0.4, 0.2, and 0 are the relative outputs, T_{tbl} . Finally, the table output is multiplied by the requested braking torque value, $T^* \equiv T_B^* \cdot T_{tbl}$.

TABLE I
LOOKUP TABLE FOR THE TABULAR CONTROL

Deceleration, a	Torque (p.u) at different front wheel slip λ					
	$\lambda < 0.06$	$\lambda < 0.08$	$\lambda < 0.11$	$\lambda < 0.13$	$\lambda < 0.20$	$\lambda \geq 0.20$
< 3.0	0.4	0.2	0	0	0	0
$3.0 - 5.5$	0.8	0.6	0.4	0.2	0	0
$5.6 - 8.5$	1.0	0.8	0.6	0.4	0.2	0
> 8.5	1.0	1.0	1.0	0.8	0.4	0

At the beginning of every cycle, the ECU monitors the inputs. Once the signal T_B^* appears, maximal braking torque is momentary applied alarming the rapid EV deceleration. This instant is used by the road analyser for detecting the top deceleration value referred to an appropriate road surface from Fig. 7. As soon as the road is estimated, optimal wheel slip for the given surface is acquired from the lookup table, and ABS is running.

After that, the slip analyser assesses an inequality of the EV and the wheel velocities. If the wheel rotates slower than the vehicle goes, the controller decreases braking torque on that wheel. The wheel then turns faster until slip achieves its optimal value. Since the wheel accelerates, torque increases again slowing down the wheel.

To understand if the surface has changed during the manoeuvre, the maximal braking torque pulse is repeatedly assigned every ABS cycle and, while torque grows, the new deceleration peak is reading for the road analyser. Thus, if the road has not been varied, approximately the same deceleration peak as in the previous step is fixed. However, if the surface is changed, the new maximal deceleration value appears. As a result, EV wheels cannot be locked even in

critical situations. They accelerate and decelerate at the same rate as the vehicle keeping wheel slip very close to the locking point. Thereby, the maximal braking power is produced allowing steering in all preliminary predicted conditions.

Despite the benefits of the tabular system, such as direct ABS orientation, high accuracy, nonlinearity, and independence of torque sensors, it has a number of drawbacks, including the requirement in careful preliminary learning, complexity of table assembling and changing, and restricted number of road surfaces and tire properties.

VI. FUZZY LOGIC CONTROLLER

To guarantee robustness of the control in every driveway, it is not enough to have information about the only dry, wet, damp, and icy surfaces. In reality, a driver deals with a variety of different environmental conditions and tire features [10], [25].

To avoid data tabulation for multiple roads and tires, the fuzzy logic module has been introduced instead of the lookup table shown in Fig. 8. The FLC designed and tuned in [23] and [24], rather than above discussed PID and tabular controllers, is capable to deal with information, which is partly true and partly false to any degree at the same time [26] (partly icy and partly wet for example). Its linguistic reasoning is applied as follows: "IF vehicle deceleration peak is somewhere between wet and icy roads, THEN keep the optimal wheel slip value somewhere between wet and icy roads". Particularly, if the road is neither wet nor icy, but the tire behaves somewhere in the middle, the amount of braking torque to keep optimal slip also might be applied somewhere between wet and icy surfaces.

The FLC designed has a multiple input, single output (MISO) topology [26]. The Mamdani's-style inference mechanism is applied (Fig. 9). The slip inputs have six triangular membership functions (MFs): MF_1 to MF_6 ; the road inputs have four MFs: icy, wet, damp, dry; whereas six triangular MFs are used to generate braking torque of different values: very high (VH), high (H), middle (M), small (S), very small (VS), and zero (Z). To keep optimal wheel slip by providing necessary braking torque on every road surface, the rule base was prepared. Table II shows this linguistic relation of 24 rules.

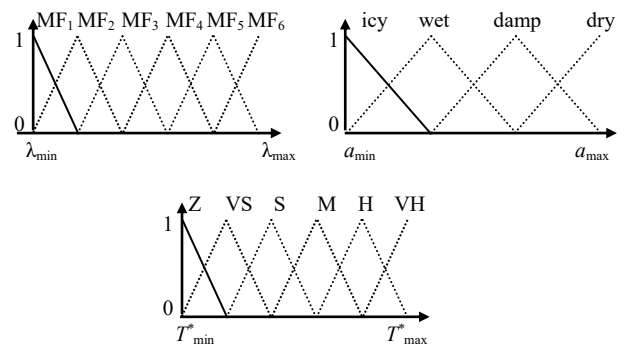


Fig. 9. Membership functions of the FLC.

TABLE II
FLC RULE BASE

Road	Torque at wheel slip MFs					
	MF_1	MF_2	MF_3	MF_4	MF_5	MF_6
icy	VS	Z	Z	Z	Z	Z
wet	M	S	VS	Z	Z	Z
damp	VH	H	M	S	VS	Z
dry	VH	VH	VH	H	S	Z

When wheel slip overcomes its optimal value, torque is reduced progressively. Once wheel slip drops, torque grows. For example, optimal wheel slip for the wet road is between 0.7 and 0.8 that is somewhere between MF_2 and MF_3 in Table II. Required torque corresponds to S or VS output values. When slip grows, torque will decrease, but as slip drops, torque rises. The same linguistic rules are true for other surfaces. For defuzzification, the centre-of-gravity approach is used.

VII. CONCLUSION

The research helps considering an influence of air friction and road inclination on braking torque distribution and accurate accounting of constraints caused by the ED and HESS. Several parts of the system, such as ECU, ABS, and tabular and fuzzy logic controllers were explored in case studies ensuring their validity and accuracy. Following the study, the FLC is proposed as the most efficient solution. It overcomes such PID drawbacks as inaccuracy at fragile and unclear road conditions, requirements in sensors, and impossibility to support equally high braking rate with time, as well as such tabular controller shortcomings as the requirement in careful preliminary learning, complexity of table assembling and changing, and restricted number of road surfaces and tire properties. In regard to ABS, the offered approach provides equally fast and safe braking with maximal energy recovery on different roads, keeping wheel slip very close to the locking point.

ACKNOWLEDGMENT

This project has received funding from the European Union's Horizon 2020 research and innovation program under grant agreement No. 675999.

REFERENCES

- [1] "Electric vehicles: Not so fast," *IEEE Spectrum*, vol. 54, no. 12, p. 24, December 2017.
- [2] J. Peng, H. He, W. Liu and H. Guo, "Hierarchical control strategy for the cooperative braking system of electric vehicle," *Scientific World Journal*, vol. 2015, no. 4, 2015, pp. 1 – 11.
- [3] X. Zhang and D. Gohlich, "A novel driving and regenerative braking regulation design based on distributed drive electric vehicles," *IEEE Vehicle Power and Propulsion Conference (VPPC)*, Hangzhou, China, 2016, pp. 1 – 6.
- [4] S. M. Savaresi and M. Tanelli, *Active Braking Control Systems Design for Vehicles*, London: Springer, 2010, 254 p.
- [5] V. Ivanov, D. Savitski and B. Shyrokau, "A survey of traction control and antilock braking systems of full electric vehicles with individually controlled electric motors," *IEEE Transactions on Vehicular Technology*, vol. 64, no. 9, pp. 3878 – 3896, September 2015.
- [6] J. Ko, S. Ko, H. Son, B. Yoo, J. Cheon and H. Kim, "Development of brake system and regenerative braking cooperative control algorithm for

- automatic-transmission-based hybrid electric vehicles," *IEEE Transactions on Vehicular Technology*, vol. 64, no. 2, pp. 431 – 440, February 2015
- [7] B. J. Varocky, *Benchmarking of Regenerative Braking for a Fully Electric Car*, Eindhoven, Netherlands: TNO Automotive, Helmond & Technische Universiteit Eindhoven, 2011, 54 p.
- [8] J. Dou, G. Cui, S. Li, X. Zhao, X. Lu and Z. Yu, "MPC-based cooperative braking control for rear-wheel-drive electric vehicle," *Chinese Automation Congress (CAC)*, Jinan, China, 2017, pp. 4419 – 4424.
- [9] P. Spichartz, T. Bokker and C. Sourkounis, "Comparison of electric vehicles with single drive and four wheel drive system concerning regenerative braking," *12th International Conference on Ecological Vehicles and Renewable Energies (EVER)*, Monte-Carlo, Monaco, 2017, pp. 1 – 7.
- [10] Y. Wang and Y. Su, "A research for brake strategy based on fuzzy control in pure electric vehicles," *4th International Conference on Computer Science and Network Technology (ICCSNT)*, Harbin, China, 2015, pp. 689 – 693.
- [11] Z. Chen, T. Lv, N. Guo, J. Shen, R. Xiao, X. Lu and Z. Yu, "Study on braking energy recovery efficiency of electric vehicles equipped with super capacitor," *Chinese Automation Congress (CAC)*, Jinan, China, 2017, pp. 7231 – 7236.
- [12] K. Itani, A. De Bernardinis, Z. Khatir, A. Jammal and M. Oueidat, "Regenerative braking modeling, control, and simulation of a hybrid energy storage system for an electric vehicle in extreme conditions," *IEEE Transactions on Transportation Electrification*, vol. 2, no. 4, pp. 465 – 479, December 2016.
- [13] F. Naseri, E. Farjah and T. Ghanbari, "An efficient regenerative braking system based on battery/supercapacitor for electric, hybrid, and plug-in hybrid electric vehicles with BLDC motor," *IEEE Transactions on Vehicular Technology*, vol. 66, no. 5, pp. 3724 – 3738, May 2017.
- [14] C. Satzger and R. De Castro, "Predictive brake control for electric vehicles," *IEEE Transactions on vehicular technology*, vol. 67, no. 2, pp. 977 – 990, February 2018.
- [15] *Regulation No 13-H of the Economic Commission for Europe of the United Nations (UN/ECE)* — Uniform provisions concerning the approval of passenger cars with regard to braking, 2015/2364.
- [16] *Brakes, Brake Control, and Driver Assistance Systems: Function, Regulation and Components*, K. Reif (Ed.), Friedrichshafen, Germany: Springer, 2014, 275 p.
- [17] M. Ehsani, Y. Gao and A. Emadi, *Modern Electric, Hybrid Electric, and Fuel Cell Vehicles: Fundamentals, Theory, and Design*, London: CRC Press, 2010, 534 p.
- [18] B. Wang, X. Huang, J. Wang, X. Guo and X. Zhu, "A robust wheel slip control design for in-wheel-motor-driven electric vehicles with hydraulic and regenerative braking systems," *American Control Conference (ACC)*, Portland, Oregon, USA, 2014, pp. 3225 – 3230.
- [19] L. Guzzella and A. Sciarretta, *Vehicle Propulsion Systems: Introduction to Modeling and Optimization*, Berlin: Springer-Verlag, 2010, 338 p.
- [20] U. Kiencke and L. Nielsen, *Automotive Control Systems: For Engine, Driveline, and Vehicle*, Berlin, Germany: Springer-Verlag Berlin Heidelberg, 2005, 521 p.
- [21] S. G. Li, S. M. Sharkh, F. C. Walsh, and C. N. Zhang, "Energy and Battery Management of a Plug-In Series Hybrid Electric Vehicle Using Fuzzy Logic," *IEEE Transactions on Vehicular Technology*, vol. 60, no. 8, pp. 3571 – 3585, October 2011.
- [22] B. K. Dash and B. Subudhi, "A fuzzy adaptive sliding mode slip ratio controller of a HEV," *IEEE International Conference on Fuzzy Systems (FUZZ-IEEE)*, Hyderabad, India, 2013, pp. 1 – 8.
- [23] A. Aksjonov, K. Augsburg and V. Vodovozov, "Design and simulation of the robust ABS and ESP fuzzy logic controller on the complex braking maneuvers," *Applied Sciences*, vol. 6, no. 12, 2016, pp. 382 – 390.
- [24] A. Aksjonov, V. Vodovozov and E. Petlenkov, "Design and experimentation of fuzzy logic control for an anti-lock braking system," *15th Biennial Baltic Electronics Conference (BEC)*, Tallinn, Estonia, 2016, pp. 207 – 210.
- [25] H. B. Pacejka, *Tyre and Vehicle Dynamics*, Oxford, UK: Butterworth-Heinemann, 2006, 672 p.
- [26] M. Negnevitsky, *Artificial Intelligence: A guide to Intelligent Systems*, Harlow, UK: Addison-Wesley, 2005, 435 p.